Available online at www.eccomasproceedia.org
Eccomas Proceedia COMPDYN (2021) 2058-2084

ECCOMAS
Proceedia

COMPDYN 2021
8th ECCOMAS Thematic Conference on
Computational Methods in Structural Dynamics and Earthquake Engineering
M. Papadrakakis, M. Fragiadakis (eds.)
Streamed from Athens, Greece, 28 - 30 June 2021

EARTHQUAKE-INDUCED STRUCTURAL POUNDING BETWEEN TWO INELASTIC SDOF STRUCTURAL SYSTEMS

Folhento P. Pedro[1], Barros C. Rui[1], and Braz-César T. Manuel[2]

[1] CONSTRUCT, Faculdade de Engenharia, Universidade do Porto
FEUP, Porto, Portugal
{up201811645, rcb}@fe.up.pt

[2] CONSTRUCT, Instituto Politécnico de Bragança
IPB, Bragança, Portugal
brazcesar@ipb.pt

Abstract

Earthquake-induced pounding among contiguous building structures with insufficient separation distance, common in highly populated areas, may generate large impact forces that can significantly modify the overall dynamic behavior of the intervenient buildings. Serious structural damage or global collapse is among the negative consequences of building pounding. Inelastic behavior is inherent in building structures subjected to moderate to severe seismic excitations. Hence, the consideration of the inelastic behavior of building structures in the occurrence of pounding is extremely important to obtain more realistic results in the study and modeling of these phenomena. To this end, a Matlab-Simulink model was developed to emulate the elastic and inelastic behavior of two lumped mass SDOF structural systems under an earthquake excitation, where pounding is likely to occur. Using a smooth hysteresis model different hysteresis cases will be considered in the inelastic behavior of the structural systems, namely, stiffness degradation, strength deterioration, and pinching effect, arising in cyclic behavior of materials that compose civil engineering structures. A non-linear viscoelastic impact model will be used to assess the magnitude of pounding forces and their relation with the interpenetration depth. It was verified that the consideration of elastic behavior in buildings prone to pounding overestimates the magnitude and number of impacts that the structures experience, and underestimates structural displacements, especially in flexible structures.

Keywords: Building pounding, Earthquake-induced structural pounding, Impact modeling, Inelastic behavior, Hysteretic model.

ISSN:2623-3347
Peer-review under responsibility of the organizing committee of COMPDYN 2021.
doi:10.7712/120121.8622.19433

1 INTRODUCTION

The world has been impacted by numerous earthquake hazard events that cause in a few amounts of time total or partial destruction of built patrimony and human activity, and potential loss of human lives. In this sense, civil and earthquake engineering came along to develop methods of analysis and design of structures, that essentially establish certain requirements to avoid the structure's collapse and minimizing damage to allow possible repair.

The seismic design of structures is primarily based on an elastic analysis to compute the seismic strength of structures. However, non-linear behavior with significant inelastic deformation is generally observed in structures under seismic events. Thus, in more advanced methods of analysis but not exclusively, this non-linear inelastic behavior can be considered in the critical zones, or plastic hinges, which within buildings are commonly located at the beams' ends, emulating in this way its behavior with an appropriate hysteresis model.

One phenomenon that has been recognized and studied for the last three decades gaining increasing importance is earthquake-induced structural pounding between adjacent buildings that are insufficiently separated.

When building pounding is likely to occur, i.e., in a situation where the buildings are very close to each other, leaving insufficient space or gaps between them or even without space, something common in metropolitan cities, great impact forces and acceleration spikes can be generated at the building floors, leading to substantial damage at the vicinity of the impact and in the worst-case scenario, it can cause the complete collapse of the structural system. Besides, and in these conditions, buildings with very different dynamic properties and consequent dynamic behavior will vibrate out-of-phase increasing the possibilities of collisions between buildings under earthquake loads.

It is known that pounding can considerably amplify the structural responses of the buildings, but in some situations, it was also found that can lead to the reduction of lateral displacements. The effects of this phenomenon are very dispersed, some in agreement, others in contradiction, while it can decrease the displacements due to the mutual blocking of the adjacent buildings it can still cause significant local damage.

And due to the high non-linearities in this contact phenomenon, pounding is very difficult to model with high accuracy since it depends on a lot of variables and their relationships. This insurgent phenomenon involves a non-linear relationship between the contact area, pressure, and deformations; local inelastic deformations; propagation of stress waves within the colliding structures; tangential and friction forces; vibrations resulting in thermal and acoustic effects; and other complex situations that makes this phenomenon extremely difficult to model.

Earthquake-induced structural pounding is usually assessed considering that the structures are within the elastic regime. This oversimplification can lead to an overestimation of the magnitude of the pounding forces and can underestimate the displacements that the structures actually experience. Some researchers already addressed this matter ([1], [2]), although additional research is required to further understand the consequences of pounding when inelastic behavior is considered.

The overall dynamic behavior of two SDOF systems with very different dynamic behavior is assessed in the following sections. These systems will represent two building structures under an earthquake excitation, in which the gap between is modified to evaluate its responses when pounding is likely to occur. The elastic and inelastic behavior of the structures will be considered. A smooth hysteresis model will be applied to emulate the non-linear hysteresis of the given structural systems.

The ultimate objective will be the understanding of the influence of the structures' non-linear inelastic behavior in the occurrence of earthquake-induced structural pounding.

2 NON-LINEAR HYSTERESIS MODEL

Hysteresis is a phenomenological concept and thus it is based on experimental data relating an input-output couple. This relationship in the present scope will represent the lateral restoring force in function of the inelastic displacement experienced by the structures.

Hysteresis is regarded as a rate-independent memory effect. However, and in reality, the response of structural systems depends always on the rate of the applied load. When this rate is significant, viscosity must be introduced. In the seismic response of structures, viscosity and hysteresis will contribute to the overall energy dissipated by the structure. Hence, the following equations of motion can be derived for the elastic and inelastic cases, respectively,

$$m\ddot{x}(t)+c\dot{x}(t)+kx(t)=-m\ddot{x}_g(t) \tag{1}$$

$$m\ddot{x}(t)+c\dot{x}(t)+ak_0x(t)+f_r^*\left[x(t),\dot{x}(t)\right]=-m\ddot{x}_g(t), \tag{2}$$

where m is the mass of the structure, c is the viscous damping, k is the elastic stiffness of the structure, $\ddot{x}_g(t)$ is the ground acceleration, $x(t)$ is the structure's displacement, $\dot{x}$ is the structure's velocity, $\ddot{x}(t)$ is the structural acceleration. Parameters k_0 and f_r^* for the inelastic case are, respectively, the initial elastic stiffness and the restoring force comprising the hysteresis stiffness and which depends on the displacements and velocities.

More realistic hysteresis models are essential to accurately characterize an inelastic response analysis of a structural system subjected to dynamic loads, such as seismic excitations. The hysteresis models in the literature can be broadly characterized in polygonal (PHM) and smooth hysteresis models (SHM).

In this study, an SHM is used. This model was initially developed by Bouc ([3]-[6]), modified by Wen ([7], [8]), and further modified by many others ([9]-[12]). The modification used herein is the one developed by Sivalselvan and Reinhorn ([13], [14]).

Figure 1 displays the scheme used in this hysteresis model. This model is capable of simulating different behaviors of a structural system under cyclic loading, viz., strength hardening, the Bauschinger effect, stiffness degradation, strength deterioration, and the pinching effect.

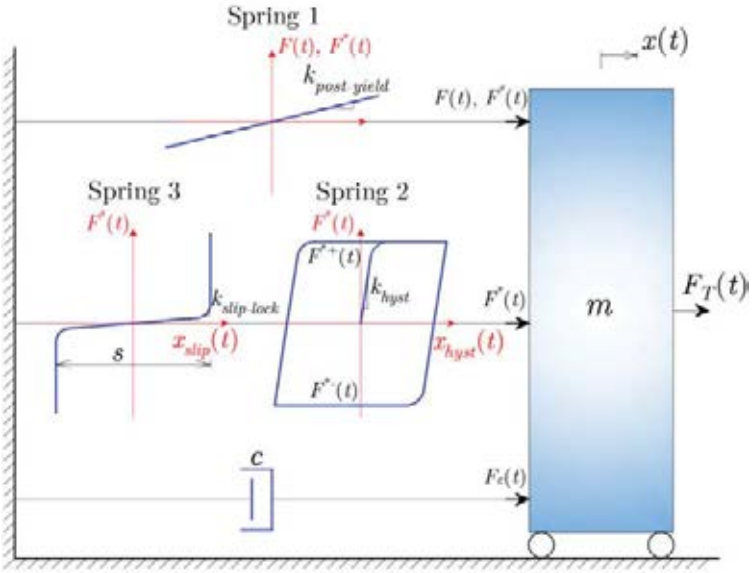

Figure 1: Sivaselvan and Reinhorn's smooth hysteresis model schematic representation.

Three different springs are used within the model: a post-yield spring (Spring 1); a hysteresis spring (Spring 2), and a slip-lock spring (Spring 3).

This modification to the original Bouc-Wen provides a more physical understanding than the previous modifications since the parameters are chosen in such a way to carry a physical meaning. A brief description of the model is presented below based on [14].

Spring 1 and Spring 2 are used in parallel to model post-yield strength hardening, and stiffness degradation, respectively. Hence, upon the application of a load, the springs undergo the same deformation, although they share this force in proportion to their instantaneous stiffness,

$$k = k_{post\text{-}yield} + k_{hyst} \tag{3}$$

in which the post-yielding stiffness, $k_{post\text{-}yield}$, is represented by a linear elastic spring (Spring 1), and the hysteresis spring, k_{hyst}, is represented by a pure elasto-plastic spring with a smooth transition from the elastic to the inelastic range (Spring 2), that may display degradation phenomena. The linear elastic stiffness and the non-degrading hysteresis stiffness are given by the following expressions, respectively,

$$k_{post\text{-}yield} = ak_0 \tag{4}$$

$$k_{hyst} = (1-a)k_0\left\{1-\left|\frac{F^*}{F_Y^*}\right|^{n_W}\left[\eta_1 \operatorname{sgn}\left(F^* dx\right)+\eta_2\right]\right\} \tag{5}$$

where a is the post to pre-yielding stiffness ratio, n_W controls the smoothness of the transition from elastic to plastic stages, η_1 and η_2 are parameters that control the shape of the unloading curve, F^* and F_Y^* are the portion of the applied force shared by the hysteresis spring and its respective yield value, which are given, respectively, by

$$F^* = (x - x_0)(1-a)k_0 \tag{6}$$

$$F_Y^* = (1-a)F_Y \tag{7}$$

To model stiffness degradation, parameter α is introduced in factor R_K which is a positive parameter with the unity as its possible maximum value. This factor is given by the following expression

$$R_K = \frac{F^* + \alpha F_Y^*}{k_0 x + \alpha F_Y^*} \tag{8}$$

is implemented in the present SHM in the hysteresis spring, in this way only the hysteresis stiffness is modified in the following way

$$k_{hyst} = (R_K - a)k_0\left\{1-\left|\frac{F^*}{F_Y^*}\right|^{n_W}\left[\eta_1 \operatorname{sgn}\left(F^* dx\right)+\eta_2\right]\right\} \tag{9}$$

To include strength deterioration a rule based on a continuous energy-based degradation, and on a backbone degradation which occurs when the maximum deformation value attained in the past is exceeded and is given by the following expression

$$F_Y^{+/-} = F_{Y0}^{+/-}\left[1-\left(\frac{x_{\max}^{+/-}}{x_{\text{ult}}^{+/-}}\right)^{\frac{1}{\beta_1}}\right]\left[1-\frac{\beta_2}{1-\beta_2}\frac{E_h}{E_{h\text{ult}}}\right] \tag{10}$$

where $F_Y^{+/-}$ is the positive or negative yield force, $F_{Y0}^{+/-}$ is the initial positive or negative yield force, $x_{\max}^{+/-}$ is the maximum positive or negative displacement, $x_{\text{ult}}^{+/-}$ is the ultimate positive or negative displacement, E_h is the hysteresis energy dissipated, $E_{h\text{ult}}$ is the hysteresis energy dissipated when loaded monotonically until the ultimate displacement without any degradation, β_1 is a parameter based on ductility demands, and β_2 is a parameter based on energy demands. The second term on the right side of Equation 10 is related to strength deterioration based on increased deformation and the last term is related to the hysteresis energy dissipated.

The hysteresis energy dissipated can be given in incremental form as follows

$$\Delta E_h = \left[\frac{F + \left(F + \Delta F\right)}{2}\right]\left(\Delta x - \frac{\Delta F}{R_K k_0}\right) \tag{11}$$

A "slip-lock" spring (Spring 3) represented in Figure 1 was implemented in the hysteresis model to simulate pinching behavior. The combined stiffness from the three springs can be given as

$$k = k_{post\text{-}yield} + \frac{k_{hyst} k_{slip\text{-}lock}}{k_{hyst} + k_{slip\text{-}lock}} \tag{12}$$

where

$$k_{slip\text{-}lock} = \left\{\sqrt{\frac{2}{\pi}}\frac{s}{F_\sigma^*}\exp\left[-\frac{1}{2}\left(\frac{F^* - F_m^*}{F_\sigma^*}\right)^2\right]\right\}^{-1} \tag{13}$$

in which s is the slip length, F_σ^* is a measure of the force range over which slip occurs, and F_m^* is the mean force level on either side about which slip occurs, being these three parameters given, respectively, as follows

$$s = R_s\left(x_{\max}^+ - x_{\max}^-\right) \tag{14}$$

$$F_\sigma^* = \sigma F_Y^* \tag{15}$$

$$F_m^* = \lambda_s F_Y^* \tag{16}$$

where parameters R_s, σ_s, and λ_s are parameters that control each of the resulting values of the previous three equations.

With the right tuned hysteresis parameters presented in Equations 3 to 16 different hysteretic behaviors can be achieved and replicated, representing different structural systems, elements, or with different materials.

3 IMPACT MODELS REVIEW

As mentioned in the introduction section, structural pounding involves different and complex phenomena that make the problem of earthquake-induced structural building pounding extremely complicated to model.

When modeling structural pounding between buildings it is enough to accurately estimate the magnitude of the pounding forces to understand how these forces will influence the overall dynamic behavior of the intervenient structures. Hence, in the literature two possible ways to model these forces are available: stereomechanics or the classical theory of impact, and the use of impact or contact elements [15].

The first approach is limited to the specification of the initial and final impact velocity states of the colliding rigid bodies (Equations 17 and 18), as well as the applied linear or angular impulse-momentum.

$$\dot{x}_{1,f} = \dot{x}_{1,0} - (1+\mathrm{CR})\frac{m_2\dot{x}_{1,0} - m_2\dot{x}_{2,0}}{m_1 + m_2} \tag{17}$$

$$\dot{x}_{2,f} = \dot{x}_{2,0} + (1+\mathrm{CR})\frac{m_1\dot{x}_{1,0} - m_1\dot{x}_{2,0}}{m_1 + m_2} \tag{18}$$

This approach cannot describe transient stresses or forces and fails to account for local deformations at the contact point of the bodies assuming that a negligibly part of the initial kinetic energy of the system is transformed into vibrations of the colliding bodies [16].

The impact velocities are related to the very important parameter, coefficient of restitution (CR),

$$\mathrm{CR} = \frac{\dot{x}_{2,f} - \dot{x}_{1,f}}{\dot{x}_{1,0} - \dot{x}_{2,0}} \tag{19}$$

in which its value represents the energy losses and degree of inelasticity of the collision being directly related with the kinetic energy loss ($-\Delta E_k$) during impact, as follows

$$-\Delta E_k = \frac{1}{2}\left(\frac{m_1 m_2}{m_1 + m_2}\right)\left(1-\mathrm{CR}^2\right)\left(\dot{x}_{1,0} - \dot{x}_{1,0}\right)^2 \tag{20}$$

A coefficient of restitution equal to one represents a perfectly elastic impact and equal to zero represents a perfectly plastic impact. This coefficient is found to be intrinsically correlated with the prior-impact velocity ([16], [17]).

The classical theory of impact is generally not used in structural pounding due to referred limitations. In addition, it neglects the existence of the period of impact failing to directly assess the evolution of the pounding forces during contact [18].

In reality, the period of impact exists and is divided into the approach (compression, loading, deformation) and restitution (unloading, elastic) periods. These periods are explicitly considered in most of the impact models that constitute the second approach available in modeling structural pounding between buildings under seismic excitations.

This approach is essentially based on a penalty method, i.e., when the buildings interpenetrate, the impact element is activated generating the pounding forces that push the structures apart. Considering the unidirectional relative displacements of the colliding structures, the impact element becomes active when

$$\delta(t) > 0 \quad \text{where} \quad \delta(t) = x_1(t) - x_2(t) - \mathrm{Gap} \tag{21}$$

in which $\delta(t)$ is the interpenetration depth of the colliding structures.

These models are compression-only zero-length elements comprising a massless spring and dashpot in parallel. The structures involving large masses can be considered as rigid bodies, having the masses lumped at the stories' levels.

The use of these elements is based on Hertz's theory and oversimplified assumptions that make the analysis of the problem simpler yet less accurate [19].

According to theories of contact mechanics [19], in impact problems, the stress wave propagation will have a significant influence on the distribution of forces within the structure. However, if one can assume that the stress waves will travel through the structures being re-

flected many times before any of them is brought to rest, then the state of stress in the structures at any instant can be considered approximately uniform throughout its length. Thus, the sudden changes in stress associated with the passage of the elastic stress waves within the structure are small compared with the general stress level. This justifies the use of the well-known spring-dashpot element with acceptable accuracy, ignoring the dynamic effects in the structures due to wave propagation and assuming that structural pounding between buildings can be approximately quasi-static if the duration of the impact is long enough to allow stress waves to transverse the length of the body many times.

In addition, the contact area is in general elliptical and is assumed to be small in comparison with the main dimensions of the bodies; deformations are restricted to the vicinity of the impact; contact surfaces are non-conforming, smooth, continuous, and frictionless; and the contact regions are assumed to remain elastic and unaltered after impact events.

During impact, the spring will control the elastic restoring force and deformation, and the dashpot will account for the energy radiated due to impact by wave motion. With these impact models is thus possible to determine with reasonable accuracy the magnitude of the impact forces at any instant during structural pounding between buildings, which is the fundamental information to understand how pounding influences the overall dynamic response of the colliding buildings.

Nonetheless, and cumulative to the oversimplified assumptions, the effectiveness of the impact models largely depends on its parameters, viz., impact stiffness and impact damping ratio. The impact stiffness (k_{imp}) namely depends on the material properties and geometric characteristics of the region of impact, and hence it presents high levels of uncertainties. The impact damping ratio (ξ_{imp}) depends mostly on the coefficient of restitution and is generally derived from energy considerations.

Based on the relations between these parameters several impact models were developed in the literature.

The most basic impact model is the linear elastic model (Figure 2a), comprising only a spring and lacking the ability to account for energy loss during impacts which is inevitable in this kind of phenomenon. The pounding force, $f_P(t)$, can then be determined by the following expression

$$f_P(t) = \begin{cases} k_{imp}\,\delta(t), & \text{for} \quad \delta(t) > 0 \\ 0 & \text{for} \quad \delta(t) \le 0 \end{cases} \tag{22}$$

The non-linear elastic model or Hertz's contact model follows Hertz's contact law [20], which describes the static compression between two isotropic elastic bodies according to the previously defined assumptions. It essentially consists of a non-linear spring as represented in Figure 2b. The spring non-linearity is capable of modeling the force-deformation relation more realistically, i.e., the contact area between neighboring structures is expected to increase as the contact force grows, leading to a non-linear stiffness. In other words, the impact force increases with the interpenetration depth to the power of 3/2 [19],

$$f_P(t) = \begin{cases} \beta_{imp}\left[\delta(t)\right]^{\frac{3}{2}} & \text{for} \quad \delta(t) > 0 \\ 0 & \text{for} \quad \delta(t) \le 0 \end{cases} \tag{23}$$

in which β_{imp} is a parameter indicating the non-linear impact stiffness depending on material properties and geometry of the colliding structures. Simplified formulae were developed by Goldsmith [16] to compute the impact stiffness parameters depending on the shape of the colliding bodies.

Alternatively, a linear viscoelastic impact model (also called Kelvin-Voigt model) as represented in Figure 2c, can be used accounting for the energy dissipation during impact ([21], [22]). The pounding force can be computed using the following system of equations

$$f_P(t) = \begin{cases} k_{imp}\,\delta(t) + c_{imp}\,\dot{\delta}(t), & \text{for} \quad \delta(t) > 0 \\ 0 & \text{for} \quad \delta(t) \le 0 \end{cases} \tag{24}$$

where c_{imp} is the damping constant of the pounding contact element computed by the following expression ([22], [23])

$$c_{imp} = 2\,\xi_{imp}\sqrt{k_{imp}\,\frac{m_1 m_2}{m_1 + m_2}} \quad \text{where} \quad \xi_{imp} = \frac{-\ln(\mathrm{CR})}{\sqrt{\pi^2 + \left[\ln(\mathrm{CR})\right]^2}} \tag{25}$$

A shortcoming to this model is the tension stress verified at the end of the restitution period, i.e., immediately before separation of the bodies, produces a negative pounding force, pulling the bodies together in the unloading phase not having a physical meaning. This happens since the parallel association in the Kelvin solid means that the total stresses are obtained as the summation of the stresses in the spring and dashpot, i.e., all elements will suffer the same deformation, meaning that the stress-strain curves produced in both periods of impact will have the same damping coefficient. This will produce a uniform dissipation of energy on both periods of impact, which in reality does not happen ([15], [16]). Also, it is observed that the elastic strain energy stored in the first period of impact is released in the second period without major plastic effects, being that most of the energy dissipated is verified to be lost in the approach period, while in the restitution period only a relatively small quantity is observed to be dissipated.

To address and solve these drawbacks some modifications to the Kelvin-Voigt impact model have been developed. Komodromos et al. [24] proposed the following modification

$$f_P(t) = \begin{cases} k_{imp}\,\delta(t) + c_{imp}\,\dot{\delta}(t), & \text{for} \quad f_P(t) > 0 \\ 0 & \text{for} \quad f_P(t) \le 0 \end{cases} \tag{26}$$

Valles and Reinhorn [25], modified the Kelvin-Voigt model by considering the damping term to be activated only for positive velocities during impact which means only activated during the approach period (Figure 2e). The following compact expression was suggested

$$f_P(t) = \left\{ k_{imp}\,\delta(t) + c_{imp}\,\dot{\delta}(t)\,H\left[\dot{\delta}(t)\right] \right\} H\left[\delta(t)\right] \tag{27}$$

where H is the unit step or Heaviside function. The expressions used to compute the impact damping coefficient and ratio are the same as in Equation 25, and an expression to compute an equivalent coefficient of restitution was derived based on the instant of time of maximum deformation (end of approach period), impact frequency (ω_{imp}), impact damped frequency ($\omega_{d,imp}$), and impact damping ratio

$$\mathrm{CR} = \sin\left(\omega_{d,imp} t_{\max}\right) \mathrm{e}^{-\xi_{imp}\,\omega_{imp}\,t_{\max}} \quad \text{where} \quad t_{\max} = \frac{1}{\omega_{d,imp}} \tan^{-1}\left(\frac{\omega_{d,imp}}{\xi_{imp}\,\omega_{imp}}\right) \tag{28}$$

Mahmoud [26] addressed the drawbacks of the linear viscoelastic impact model by redefining the pounding force depending on the two periods of impact. The author considered a similar approach to Valles and Reinhorn [25] (Figure 2e), and the following equivalent expression was suggested

$$f_P(t)=\begin{cases} k_{imp}\,\delta(t)+c_{imp}\,\dot{\delta}(t) & \text{for} \quad \delta(t)>0, \quad \dot{\delta}(t)>0 \\ k_{imp}\,\delta(t) & \text{for} \quad \delta(t)>0, \quad \dot{\delta}(t)\le 0 \\ 0 & \text{for} \quad \delta(t)\le 0, \end{cases} \tag{29}$$

The relationship between the damping ratio and the CR was reevaluated since the energy dissipation properties depend on the damping term, which now is only active in the first period of impact. The author used the same procedure as Jankowski in [27] using energy considerations, arriving at the following expression

$$\xi_{imp}=\frac{1}{\pi}\frac{1-\mathrm{CR}^2}{\mathrm{CR}} \tag{30}$$

Ye et al. [28] proposed the following modification to the Kelvin-Voigt model (Figure 2e) at the impact damping coefficient and ratio

$$c_{imp}=\xi_{imp}\delta(t) \quad \text{where} \quad \xi_{imp}=\frac{3k_{imp}(1-\mathrm{CR})}{2\mathrm{CR}\left(\dot{x}_{1,0}-\dot{x}_{2,0}\right)}. \tag{31}$$

Pant et al. ([29], [30]) developed a modification on the Kelvin-Voigt impact model (Figure 2e) considering the same expression presented by Mahmoud in Equation 29, by modifying the expression of the impact damping ratio as follows

$$\xi_{imp}=\frac{3k_{imp}\left(1-\mathrm{CR}^2\right)}{2\mathrm{CR}^2\left(\dot{x}_{1,0}-\dot{x}_{2,0}\right)} \tag{32}$$

Following the research in Mahmoud [26], Mahmoud and Jankowski [31] suggested a further modification to the linear viscoelastic model (Figure 2e) using a different approach to arrive at an improved formula for the impact damping ratio

$$\xi_{imp}=\frac{1-\mathrm{CR}^2}{\mathrm{CR}\left[\mathrm{CR}(\pi-2)+2\right]} \tag{33}$$

In the modifications to the Hertz contact model, the lack of energy dissipation properties was addressed by the addition of non-linear damping becoming now a non-linear viscoelastic model. Lankarani and Nikraves ([32], [33]) proposed a contact model considering a non-linear spring using Hertz's law in parallel with non-linear damping in hysteresis form proposed by Hunt and Crossley [34] (Figure 2d) to better represent impacts between mechanical systems. The authors considered the pounding force to be computed as follows

$$f_P(t)=\beta_{imp}\left[\delta(t)\right]^n+c_H\dot{\delta}(t) \tag{34}$$

where c_H is the non-linear damping coefficient given by

$$c_H=\mu_d\left[\delta(t)\right]^n \quad \text{where} \quad \mu_d=\frac{3\beta_{imp}\left(1-\mathrm{CR}^2\right)}{4\left(\dot{x}_{1,0}-\dot{x}_{2,0}\right)}\dot{\delta}(t) \tag{35}$$

in which μ_d is the hysteresis damping factor and n=3/2 to represent Hertz's law. Muthukumar and DesRoches ([35], [36]) proposed an impact model, the "Hertzdamp" impact model represented in Figure 2d, using the previous considerations applied to civil engineering structures

$$f_P(t)=\begin{cases}\beta_{imp}\left[\delta(t)\right]^{\frac{3}{2}}+c_H\,\dot{\delta}(t) & \text{for} \quad \delta(t)\geq 0\\ 0 & \text{for} \quad \delta(t)<0\end{cases} \tag{36}$$

where the impact damping ratio is now

$$\xi_{imp}=\frac{3\beta_{imp}\left(1-\mathrm{CR}^2\right)}{4\left(\dot{x}_{1,0}-\dot{x}_{2,0}\right)}\dot{\delta}(t) \tag{37}$$

Jankowski [37] proposed a modification to Hertz's non-linear impact model by considering that the non-linear damping component is only active in the approach period (Figure 2f) since it is in this period of the impact that most energy is dissipated. Thus, the pounding force is obtained using the following piecewise function

$$f_P(t)=\begin{cases}\beta_{imp}\left[\delta(t)\right]^{\frac{3}{2}}+c_H(t)\dot{\delta}(t) & \text{for} \quad \delta(t)>0 \quad \text{and} \quad \dot{\delta}(t)>0\\ \beta_{imp}\left[\delta(t)\right]^{\frac{3}{2}} & \text{for} \quad \delta(t)>0 \quad \text{and} \quad \dot{\delta}(t)\leq 0\\ 0 & \text{for} \quad \delta(t)\leq 0\end{cases} \tag{38}$$

The impact element's damping can be considered as an extension of the linear viscoelastic model (modified Kelvin-Voigt) and is obtained with the following expression

$$c_H(t)=2\xi_{imp}\sqrt{k_{imp}\frac{m_1m_2}{m_1+m_2}} \quad \text{where} \quad k_{imp}=\beta_{imp}\sqrt{\delta(t)} \tag{39}$$

The second of Equation 39 can be seen as an effective impact stiffness for a given value of the interpenetration depth. Additionally, Jankowski ([27], [37]) redefined the expression for the damping ratio which is related to the coefficient of restitution since now the non-linear damping is only active in the approach period. To do this the author developed two algebraic expressions (with approximating functions) for the impact damping ratio and then compared them with numerical results to verify its validity. The two expressions are

$$\xi_{imp}=\frac{\sqrt{5}}{2\pi}\frac{1-\mathrm{CR}^2}{\mathrm{CR}} \quad \text{and} \quad \xi_{imp}=\frac{9\sqrt{5}}{2}\frac{1-\mathrm{CR}^2}{\mathrm{CR}\left[\mathrm{CR}\,(9\pi-16)+16\right]} \tag{40}$$

in which the second was found to provide better approximations. The approximating functions used by Jankowski in [27] served as the base to the procedure adopted by Mahmoud and Mahmoud and Jankowski in [26] and [31], respectively. Also, the results regarding the relationship between the impact damping ratio and the coefficient of restitution in impact models drew attention to the fact that when the coefficient of restitution becomes zero the impact damping ratio should go to infinity. This was addressed by Ye et al. [28] for the modification to the original Kelvin-Voigt that provided the unit value of the impact damping ratio for zero value of the coefficient of restitution, and by the same authors [38] for the modification of the Hertzdamp model that gave a finite value for the impact damping ratio for perfectly plastic collisions. Besides, all models corroborated the fact that a coefficient of restitution of one corresponds to the obvious zero value of the impact damping ratio.

Ye et al. [38] then arrived at a more accurate expression to approximate the damping constant given by

$$\xi_{imp} = \frac{8\,\beta_{imp}\,(1-\mathrm{CR})}{5\mathrm{CR}\left(\dot{x}_{1,0}-\dot{x}_{2,0}\right)} \tag{41}$$

which confirms the aforementioned premises by Jankowski [27] and was then validated through numerical simulations.

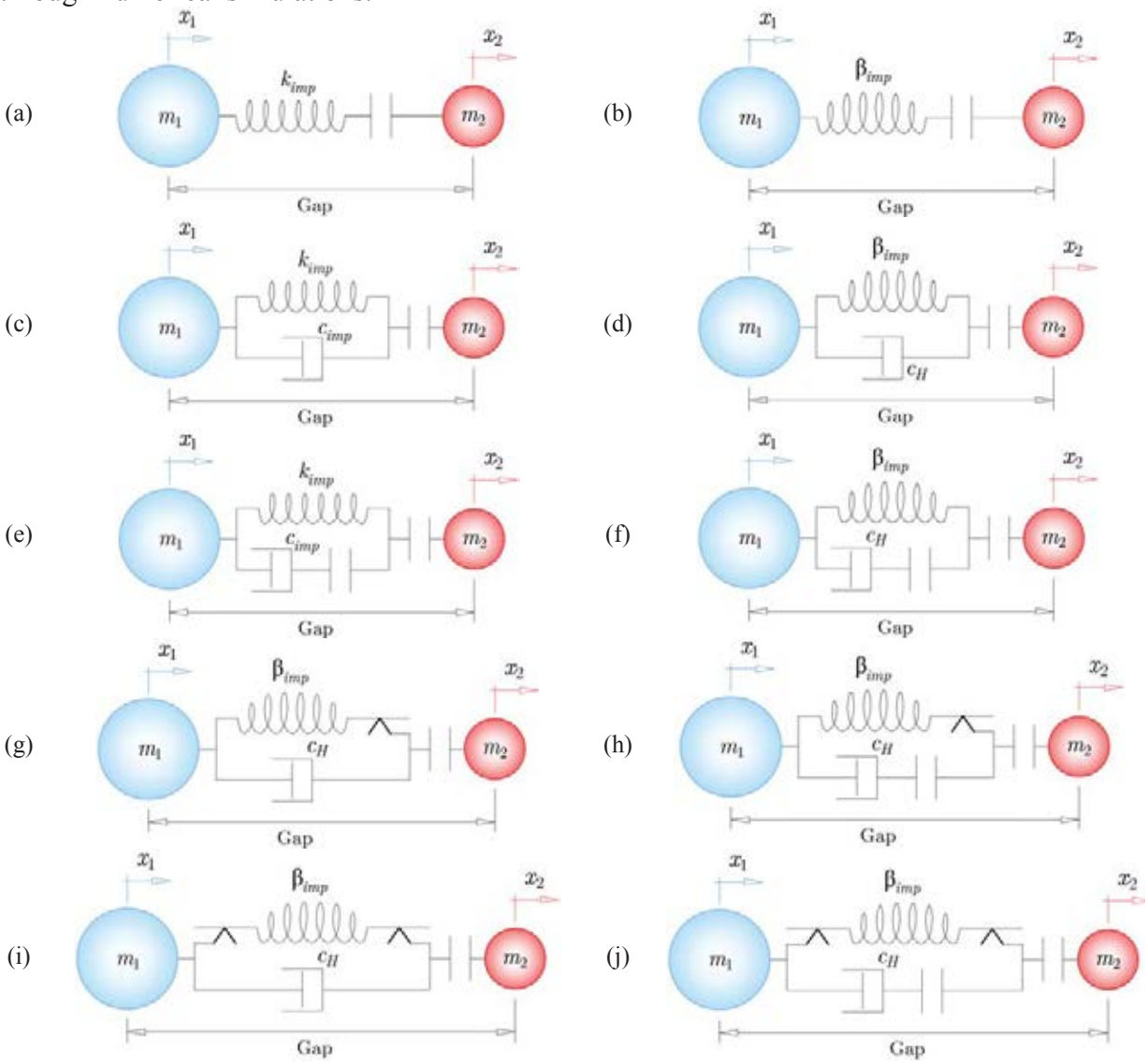

Figure 2: Schematic representation of state-of-the-art impact models.

More recently, Naderpour et al. [39] considered an equivalent expression to Equation 34 and the first of Equation 35 to compute the pounding force between buildings. Ultimately, a new expression for the impact damping ratio for the non-linear viscoelastic model (Figure 2f) related to the coefficient of restitution was obtained by an iterative procedure that attempts to equate the energy dissipated by the non-linear damping in the approach period (translated by the area of the impact hysteresis loop) to the kinetic energy loss (of the stereomechanical impact), resulting in

$$\xi_{imp} = \left[\frac{2}{\mathrm{CR}\sqrt{\pi}}\left(1-\mathrm{CR}^2\right)\right]^2 \tag{42}$$

A further study by Naderpour et al. [40] suggested a new expression (see Equation 43) for the impact damping coefficient that depends on the prior-impact velocity and coefficient of restitution.

$$c_{imp}\left(t\right)=\alpha\frac{\mathrm{CR}^{\beta}\dot{\delta}_{imp}\left(1-\mathrm{CR}\right)}{\ddot{\delta}\left(t\right)}k_{imp}\delta^{n}\left(t\right) \tag{43}$$

Bamer [41] and Bamer and Markert [42], respectively, proposed an extension to the Hertzdamp and Jankowski's non-linear viscoelastic model by including a dry friction element in series with the non-linear spring (Figure 2g and 2h) to address one of the mentioned oversimplified assumptions, the unaltered contact surface which is tacitly known to experience damage and material dissipation caused by numerous and repeated impacts. The authors modified the condition of collision (see Equation 21), first by considering the equivalent condition of collision when $\delta<0$ (when the Gap is added instead of subtracted) and then by including an additional increase in the gap due to damage, material loss, or plastic deformation, yielding

$$\delta_{\mathrm{T}}\left(t\right)=\delta\left(t\right)+\delta_{s}\left(t\right)<0 \quad \text{where} \quad \delta\left(t\right)=x_{1}\left(t\right)-x_{2}\left(t\right)+\mathrm{Gap} \tag{44}$$

in which the non-negative parameter δ_s is the additional offset to the position of the initial pounded surface. Three states were then considered within the periods of impact: state 0 refers to the case without impact; state I corresponds to the activation of the impact model satisfying the condition in Equation 44; state II when a limit value of the elastic Hertz's contact force is exceeded (sliding). A constant friction force R obeying Coulomb's friction law is considered based on the material and geometric properties of the colliding surfaces, together with the non-linear damping term. An additional state, state III considered in the case of Jankowski's non-linear viscoelastic model, where the damping term is no longer active in the restitution period. Equations 45 represents, the improved models of Hertzdamp and Jankowski's non-linear viscoelastic model, according to the states defined ([41], [42])

$$f_{P}\left(t\right)=\begin{cases} f_{k}+f_{c} & \text{for} \quad \delta_{\mathrm{T}}\left(t\right)<0 \quad \text{and} \quad \dot{\delta}_{\mathrm{T}}\left(t\right)<0 \quad \text{and} \quad f_{k}<f_{R} & (\text{State I}) \\ f_{R}+f_{c} & \text{for} \quad \delta_{\mathrm{T}}\left(t\right)<0 \quad \text{and} \quad \dot{\delta}_{\mathrm{T}}\left(t\right)<0 \quad \text{and} \quad f_{k}\geq f_{R} & (\text{State II}) \\ f_{k} & \text{for} \quad \delta_{\mathrm{T}}\left(t\right)<0 \quad \text{and} \quad \dot{\delta}_{\mathrm{T}}\left(t\right)\geq 0 & (\text{State III}) \\ 0 & \text{for} \quad \delta_{\mathrm{T}}\left(t\right)\geq 0 & (\text{State 0}) \end{cases} \tag{45}$$

$$\text{where} \quad f_{k}=\beta_{imp}\left[\left|\delta\left(t\right)\right|-\delta_{s}\left(t\right)\right]^{\frac{3}{2}}, \quad f_{c}=c_{H}\left(t\right)\dot{\delta}_{\mathrm{T}}\left(t\right), \quad f_{R}=-\mathrm{sgn}\left(\dot{\delta}_{\mathrm{T}}\left(t\right)\right)R$$

Later Bamer et al. [43] went further to include in the previous model a decrease in the stiffness depending on the sliding gap which now is divided into two and attributed to each frame. A simple damage curve was then assumed to allow structural damage description. The impact model may then be represented, respectively, for the modified Hertzdamp and Jankowski's non-linear viscoelastic model in Figures 2i and 2j.

Khatami et al. [44] developed an effective formula for the impact damping ratio included in the non-linear viscoelastic impact model (Figure 2f). The authors used a program developed called the Coefficient of Restitution-Velocity-Stiffness (CRVK), which performs several dynamic analyses and solves impact problems. The accuracy of this new formula was assessed based on four different approaches that include energy-based considerations, numerical simulations, and comparisons with experimental results. The expression proposed by the authors is

$$\xi_{imp} = \frac{(1-\mathrm{CR})}{\mathrm{CR}^{(\alpha+0.204)} + 3.351\pi\,\mathrm{CR}} \mathrm{CR}^{0.204} \quad \text{where} \quad \alpha = 1.05\,\mathrm{CR}^{0.653} \tag{46}$$

Based on the previous studies regarding impact models it is possible to verify that the main modifications are at the parameters impact stiffness and impact damping ratio. These parameters along with the coefficient of restitution, which generally is the only independent variable of the impact damping ratio constitute the core of the impact models and its accuracy depends on how accurate is the estimation of these parameters.

Some experimental tests regarding pounding between structures have been carried out ([17], [45]-[49]) essentially concerning reduced-scale models. These experimental tests motivated several investigations comparing the effectiveness of the previous impact models and other comparisons between them.

For instance, based on different experimental results available in the literature regarding pounding-involved structural responses, Jankowski [37] made comparisons between Jankowski's non-linear viscoelastic model, Kelvin-Voigt model, and Hertz's non-linear model. The author verified that the Kelvin-Voigt and the non-linear viscoelastic model gave the smallest simulation errors in the pounding force time-histories during impact and that further research confirmed that Jankowski's model provided smaller errors in the response time-histories with the structural pounding.

Jankowski and Mahmoud ([15], [17]) performed experimental tests based on dropping different balls of different materials (steel, concrete, timber, and ceramic), and on the impact between reduced-scale models excited by shake tables. The results corroborated with the study addressed in the previous paragraph and revealed that the improved version of the linear viscoelastic model by Jankowski and Mahmoud did not lead to increased accuracy and that the Hertzdamp also furnished small errors in the response time-histories of earthquake-induced structural pounding.

Bamer et al. ([41]-[43]) proposed a new strategy using state-of-the-art impact models that includes damage description and failure of the pounding-involved structures. The authors verified through sensitivity analysis the importance of the consideration of the damage state of the adjacent structures.

Khatami et al. [44] compared their impact damping ratio formula with the ones of different impact models in the literature and based on different experimental tests and numerical simulations, presenting the lowest errors and proving its accuracy in the study of earthquake-induced structural pounding.

Still, most of the impact models in the literature lack the ability to emulate structural pounding between three-dimensional structures. The central impact is defined as the collision between two non-rotating objects at a point belonging to a line that connects the two centroids. An oblique impact considering a two-dimensional impact model may be possible to develop to emulate three-dimensional pounding that considers in addition to the two directions of translation of the buildings, their rotation. One good example is the model developed by Polycarpou et al. [50] that considers tangential forces and friction during impact, and the material properties and geometry of the contact area without the need to previously determine the location of the impact. The model proved to furnish good results and close to the results obtained with commercial software.

4 NUMERICAL MODELING

Two adjacent structural systems will be considered in this earthquake-induced structural pounding study, one flexible building, and the other building stiffer as represented in Figure 3.

The structures are assumed to be in shear configuration, and thus can be reduced to lumped mass models with the masses lumped at the floor levels. The structural properties of the representative buildings are considered to be the same as in [15] and are summarized in Table 1.

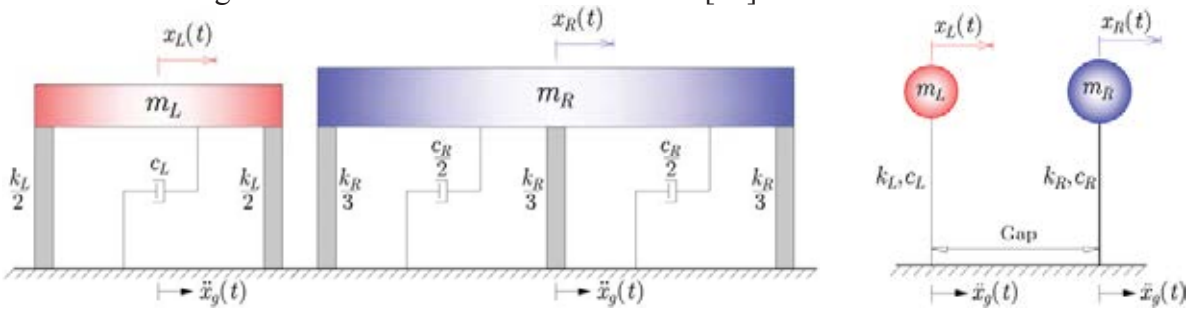

(a) Example of representation of frames in shear configuration. (b) Lumped mass models.

Figure 3: Representation of the two SDOF structural systems separated by a gap size.

Structural properties	Flexible building	Stiffer building
Mass (kg)	m_L=75000	m_R=3000×10^3
Stiffness (kN/m)	k_L=2056	k_R=1.316×10^6
Natural period (s)	T_L=1.2	T_R=0.3
Damping coefficient (kg/s)	c_L=39270	c_R=6.283×10^6
Damping ratio (%)	ξ_L=5	ξ_R=5

Table 1: Structural properties of the adjacent buildings.

Among the different types of building pounding, impacts will be assumed to happen exclusively between floors. The impact model used in this study is the one developed by Jankowski ([27], [37]), the non-linear viscoelastic model which is illustrated in Figure 2f, and so the expressions to be used are Equations 38, 39 and the second of 40. These expressions are then implemented in the equations of motion in Equations 1 and 2, being modified, respectively, for the elastic and inelastic case as follows

$$m\ddot{x}(t)+c\dot{x}(t)+kx(t)+f_P(t)=-m\ddot{x}_g(t) \tag{47}$$

$$m\ddot{x}(t)+c\dot{x}(t)+ak_0x(t)+f_r^*\left[x(t),\dot{x}(t)\right]+f_P(t)=-m\ddot{x}_g(t), \tag{48}$$

Depending on the structural behavior one of the two previous equations will be solved for each building. The term regarding the pounding force becomes activated when the buildings interpenetrate satisfying Equation 21.

The stiffness of the impact element is usually taken as the same order of magnitude as the axial stiffness of the stiffer story. This parameter depends on the geometry of the impact surfaces, material properties, variable impact velocities, and uncertainties concerning its value arising from these factors [22]. Goldsmith [16] referred that for steel-to-steel impacts the impact stiffness generally takes higher values than concrete-to-concrete impacts. Van Mier et al. [45] experiments reveal that impacts between concrete bodies depend mostly on the contact surface geometry and ranges typically between 40 $kN/mm^{3/2}$ and 80 $kN/mm^{3/2}$ (respectively, 1.2×10^9 $N/m^{3/2}$ and 2.6×10^9 $N/m^{3/2}$). Cole et al. [51] refer that the impact stiffness is typically set as ten times the stiffness of the larger axial floor.

The values used for the impact stiffness and the coefficient of restitution are, respectively, 2.75×10^9 $N/m^{3/2}$ and 0.65. These values were provided by Jankowski [37] based on comparisons between numerical simulations using the author's non-linear viscoelastic model and experimental data available in the literature.

The hysteresis parameter values considered for the present study are: a=0.1; $\eta_1=\eta_2$=0.5; α=4; β_1=0.30; β_2=0.15; σ_s=0.2; R_s=0.1; λ_s=0; n_W=3. In addition, the yield force and displacement of the left building are, respectively, F_{YL}=70 *kN*, x_{YL}=3.4 *cm*, the yield force and displacement of the right building are, respectively, F_{YR}=7000 *kN*, x_{YR}=0.53 *cm*, and the ductility is μ=10. The values were chosen according to the information furnished in [14] and are intended to be representative of a reinforced concrete (RC) frame, although the values are not the result of direct calibration with experimental data. Hence, for the RC frame a severe stiffness degradation, moderate strength deterioration, and mild to moderate pinching effect.

A Matlab/Simulink [52] model was developed and used to emulate structural pounding between the elastic and inelastic SDOF systems under the El Centro earthquake represented in Figure 4. The simulations were performed for the following values of the gap between the adjacent structures: 0 *cm*, 3 *cm*, 5 *cm*, 10 *cm*, and 15 *cm*. To solve the differential equations of motion the Runge-Kutta of 4th order was used with a fixed time step of $5\times10^{-4}s$.

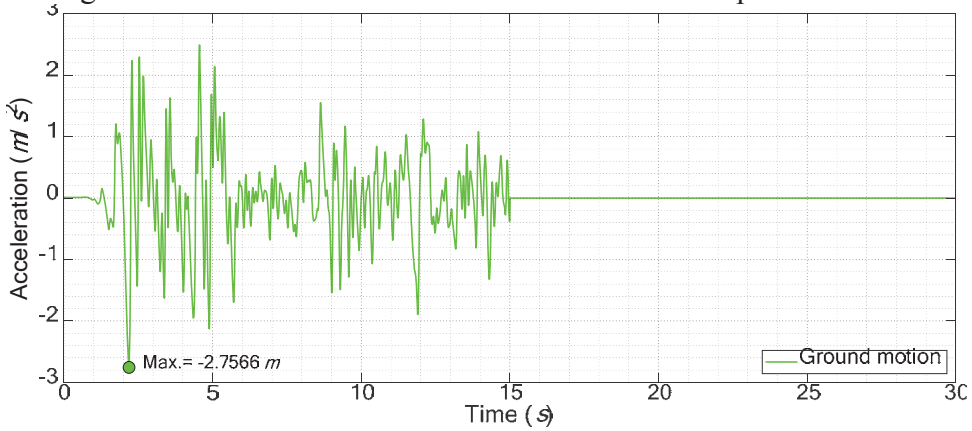

Figure 4: NS component of El Centro seismic accelerations - Station: El Centro, CA - Sta9; Imperial Valley-02 [53].

5 RESULTS AND DISCUSSION

As an example, the following results in form of graphs are presented only for the situations where the buildings have no gap in between and are separated by 3 *cm* and for the elastic and inelastic structural systems described in the previous section. Nevertheless, and for the purpose of comparisons Table 2 presents the peak responses (displacements, velocities, accelerations, and pounding forces and number of impacts) of both buildings for the different situations of the separation distance and structural behavior cases. It should be pointed out that in the case where the gap is 10 *cm* and the structural system has inelastic behavior no impacts were verified and so its response is the same as for the case with 15 *cm* of gap size, thus its results do not explicitly appear in the table.

Hence, Figures 5 to 8 present the displacement and pounding force time-history responses for the 0 *cm* and 3 *cm* of gap size and for the elastic and inelastic case. Correspondingly the graphs of Figure 9 present the pounding force vs interpenetration depth cycles for the 0 *cm* and 3 *cm* of gap size for the elastic and inelastic case. Figures 10 and 11 present comparisons between the displacements and impact forces time-history responses for the different gap sizes considered (except for the 10*cm* for the mentioned reason).

The graphs of Figures 12 and 13 present the hysteresis cycles of the left and right structural systems obtained with the aforementioned hysteresis model for the two gap cases considered, respectively.

Additionally, the acceleration time-history responses are also presented in Figures 14 to 18 for the mentioned cases to assess the acceleration spikes.

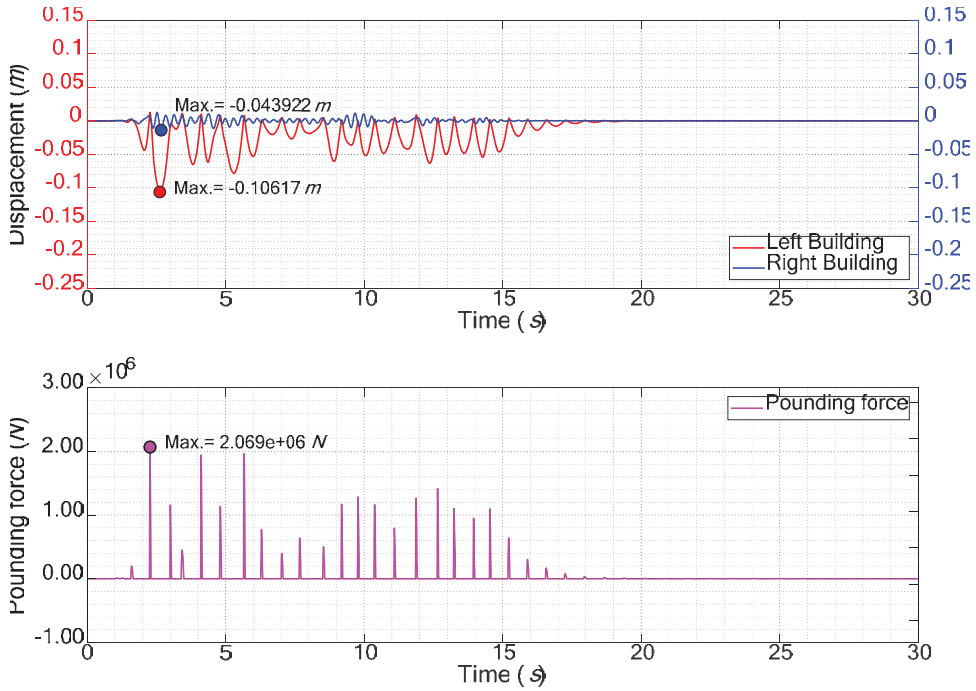

Figure 5: Displacements and pounding forces time-history responses for the elastic case of the representative structural systems with no gap in between.

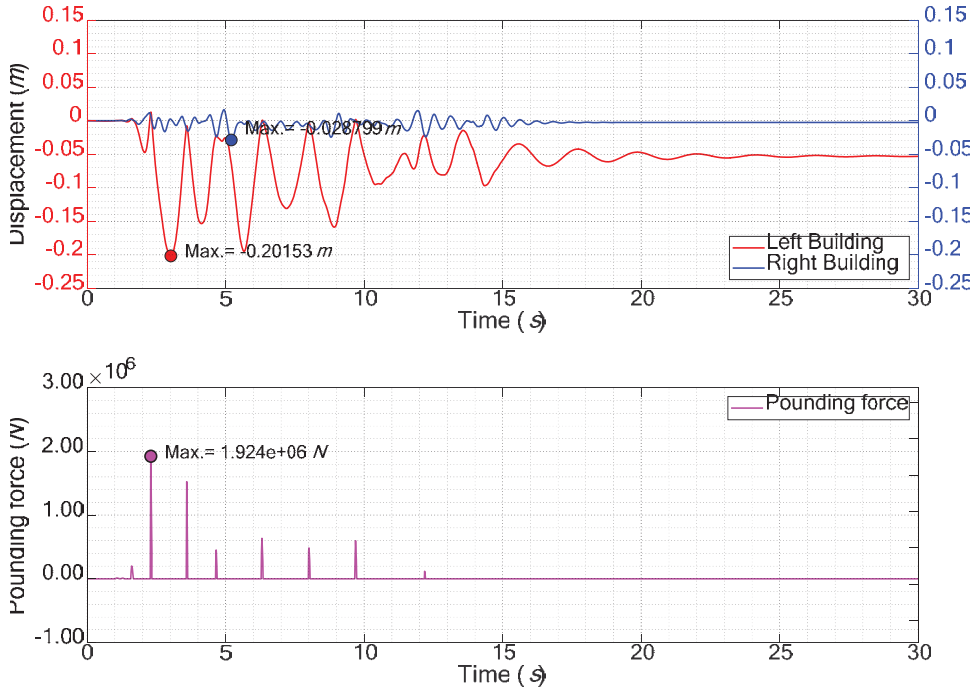

Figure 6: Displacements and pounding forces time-history responses for the inelastic case of the representative structural systems with no gap in between.

The huge differences in stiffness and mass of the structures allow for better conclusions regarding the effects of pounding between these buildings. In general, and as expected, it can be verified for every response considered that the most flexible structure is the most affected, and thus, the most sensitive to the ground motion excitation and the pounding forces.

In general, as the gap between the buildings decreases, the number of impacts increases. No distance between buildings with very different dynamic properties may constitute one of

the worst situations when pounding is likely to occur. This situation presents the biggest number of impacts between the buildings, and the intensity of the pounding forces is closer to the maximum verified in the situation with a 3 *cm* of gap size.

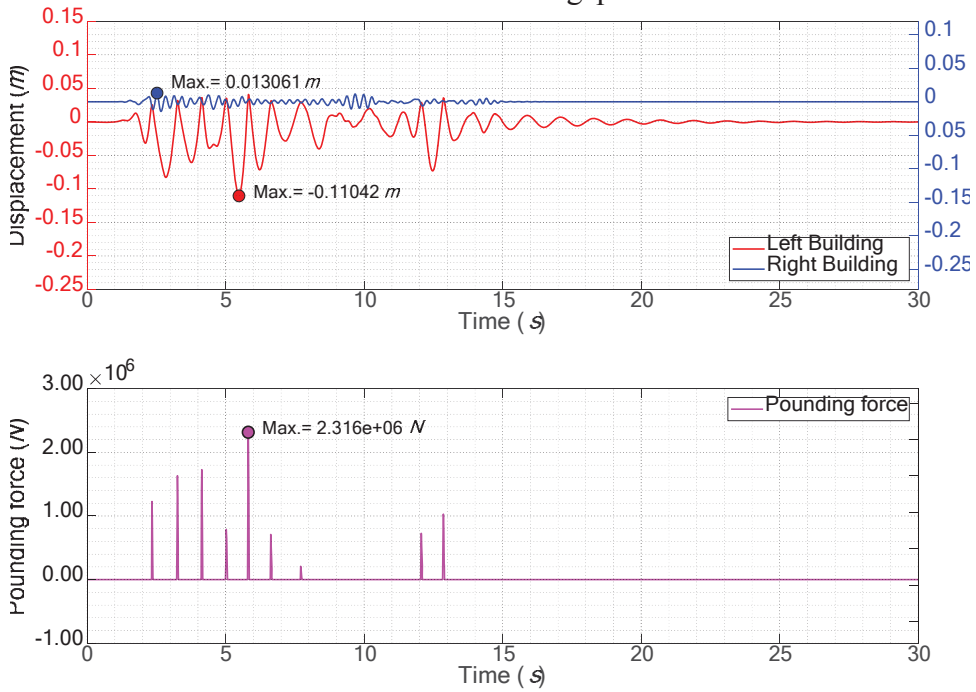

Figure 7: Displacements and pounding forces time-history responses for the elastic case of the representative structural systems separated by a distance of 3 *cm*.

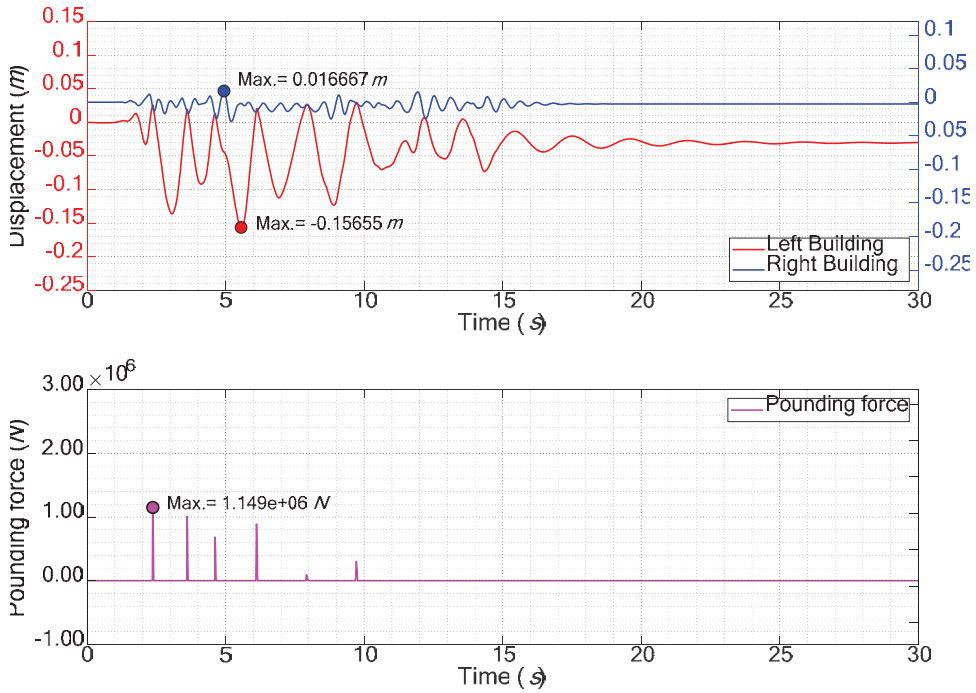

Figure 8: Displacements and pounding forces time-history responses for the inelastic case of the representative structural systems separated by a distance of 3 *cm*.

Attention should be drawn to the acceleration spikes, that in comparison with no pounding display huge percentages of increase. The sudden changes in the velocity response of the

buildings due to impacts cause these short-duration acceleration spikes in the opposite direction that can cause greater damage to the buildings' structures and contents. The graphs of Figures 14 to 17 show these acceleration spikes due to pounding between the building during the seismic hazard event.

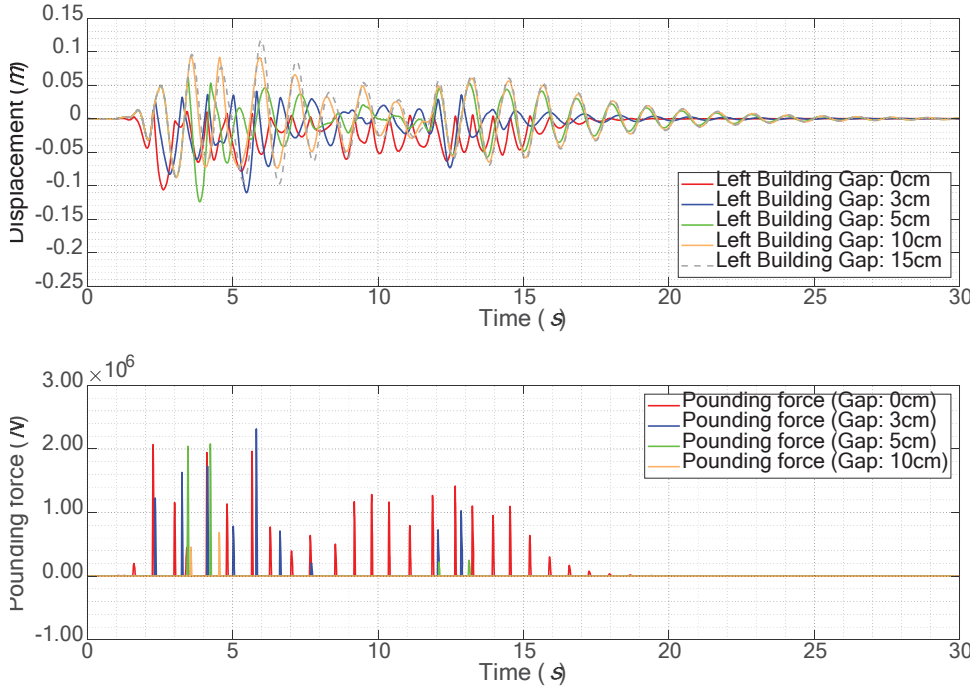

Figure 9: Comparison of the displacements and pounding forces time-history responses for the elastic case of the left building for different gap sizes.

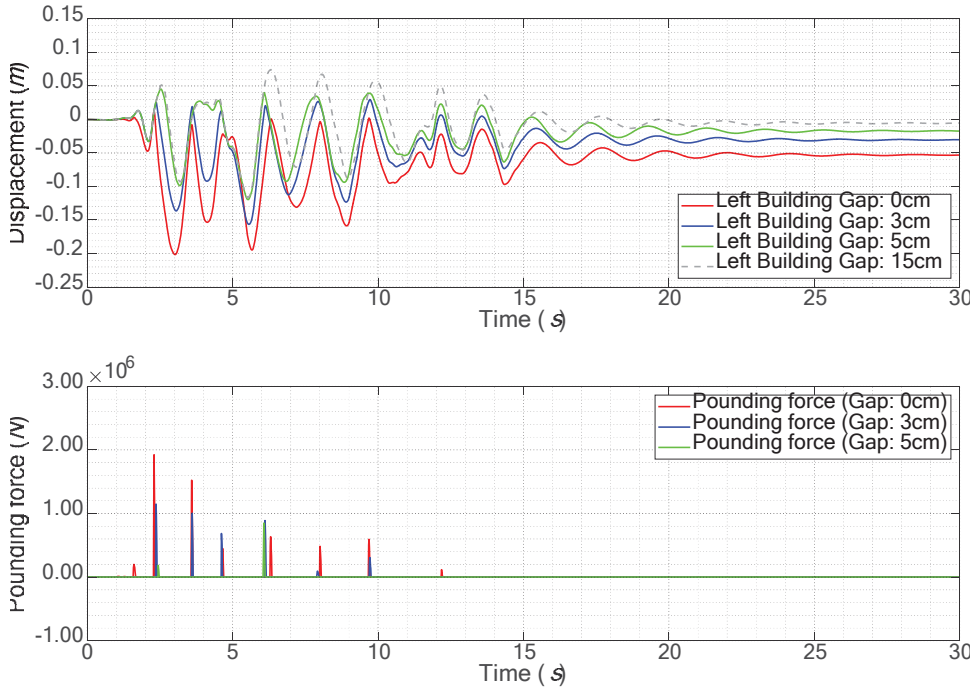

Figure 10: Comparison of the displacements and pounding forces time-history responses for the inelastic case of the left building for different gap sizes.

Observing the elastic case (Figure 5, 8, and 9) it can be seen that the mutual blocking of the buildings explains the peak displacement reductions in Table 2. It is known that pounding tends to reduce the inbound structural displacements due to building blocking. Conversely, it tends to increase the rebound displacements. This is evident in the flexible structure as can be seen in Figure 9, although the same cannot be verified in the stiffer building which experiences great reductions in the peak structural displacements (Table 2). In terms of peak velocities, the flexible structure tends to suffer increases (gap sizes of 10 *cm* and 5 *cm*), and the stiffer structure only experiences a slight decrease in the case of no separation distance. It should be stated that although there is a reduction in the peak responses when pounding is considered, this is not beneficial since great local damages at the regions of impact are implicitly known and damage in the structures due to structural inelastic behavior should be expected and aggravated due to pounding, as will be discussed in the next paragraphs.

The inelastic behavior of the structural systems has a significant influence on the structural overall dynamic behavior. As can be seen by comparing Figures 9 and 10, the inelastic case experiences fewer impacts and its intensity is also smaller. However, the presence of permanent deformations is inevitable and increases with decreasing gap size. In addition, the rebound displacements are also increased concerning the elastic case, particularly, in the flexible structure for the gap sizes of 0 *cm* and 3 *cm* since in the corresponding 5 *cm* of gap size a reduction is verified. In the case of the stiffer structure, permanent deformations are still expected although much smaller than in the flexible structure, increases were verified in the gap sizes of 3 *cm* and 5 *cm* and a decrease in the case with no gap.

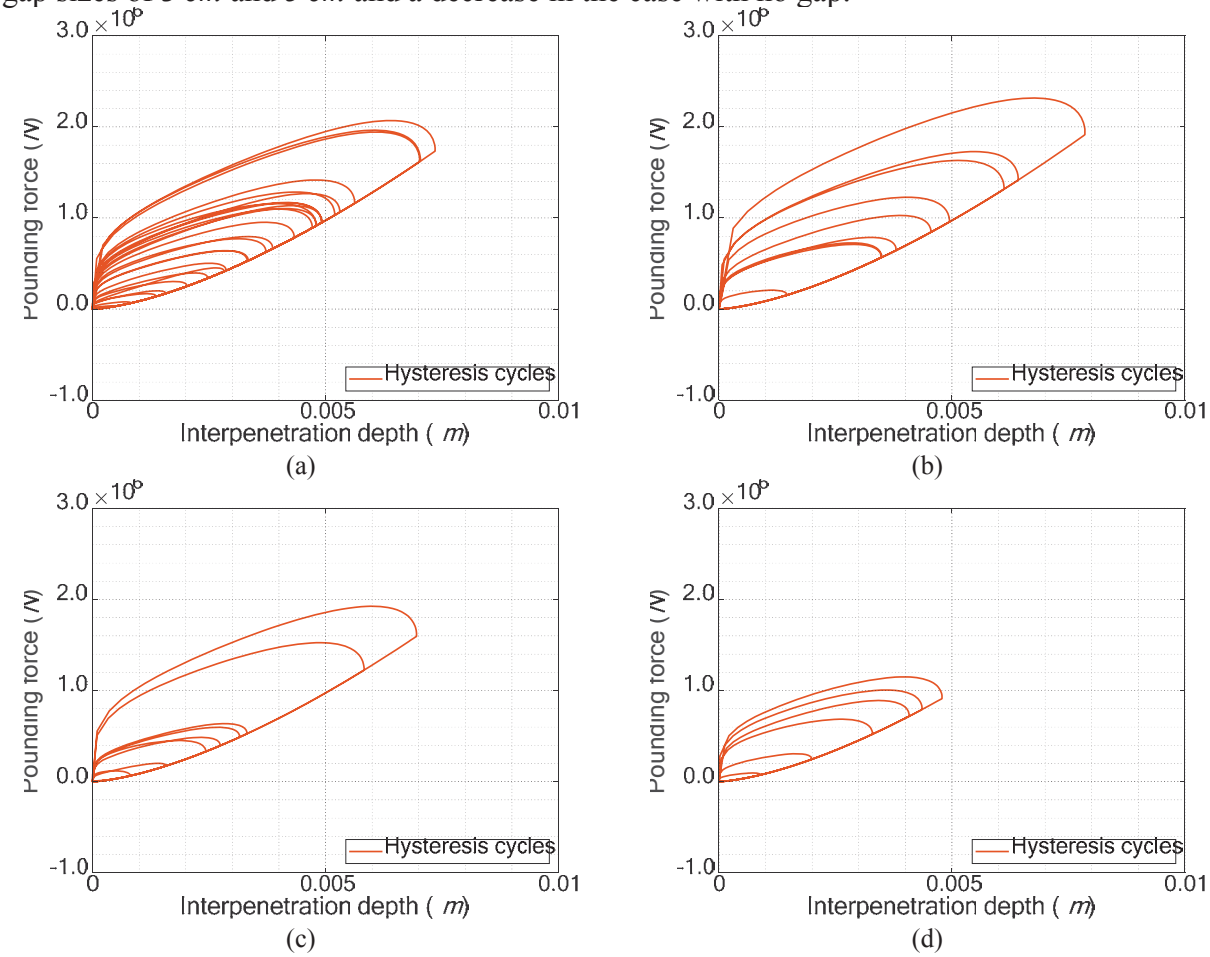

Figure 11: Pounding cycles for the elastic case of the structural systems: (a) 0 *cm*, (b) 3 *cm*; and for the inelastic case of the structural systems: (c) 0 *cm*, (d) 3 *cm*.

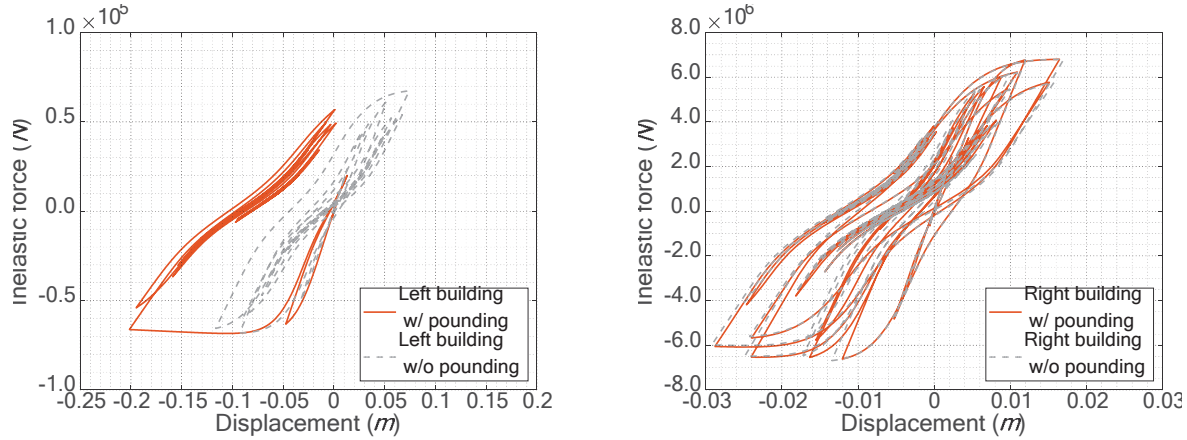

Figure 12: Hysteresis cycles when the structural systems have no gap in between: (a) Left and (b) Right building.

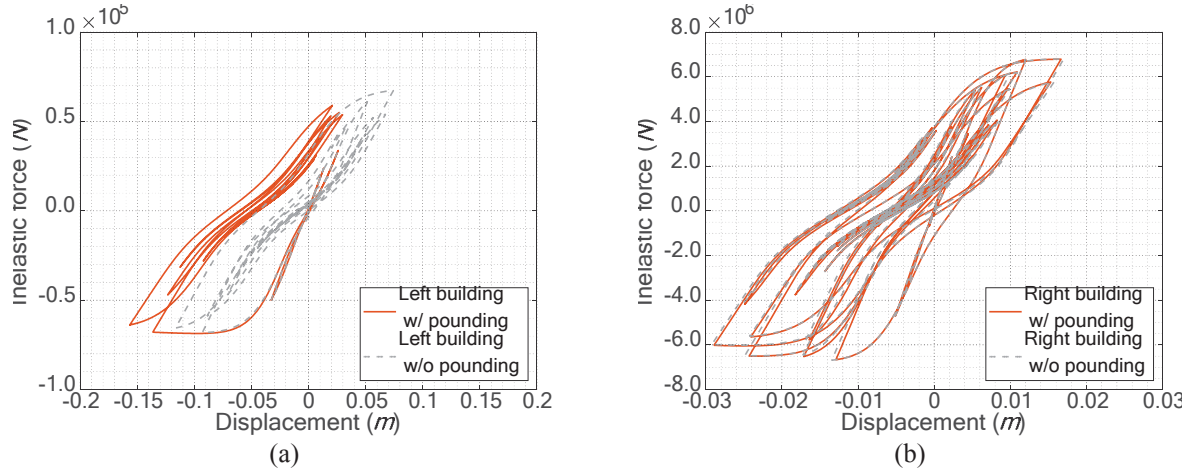

Figure 13: Hysteresis cycles when the structural systems are separated by a distance of 3 *cm*: (a) Left and (b) Right building.

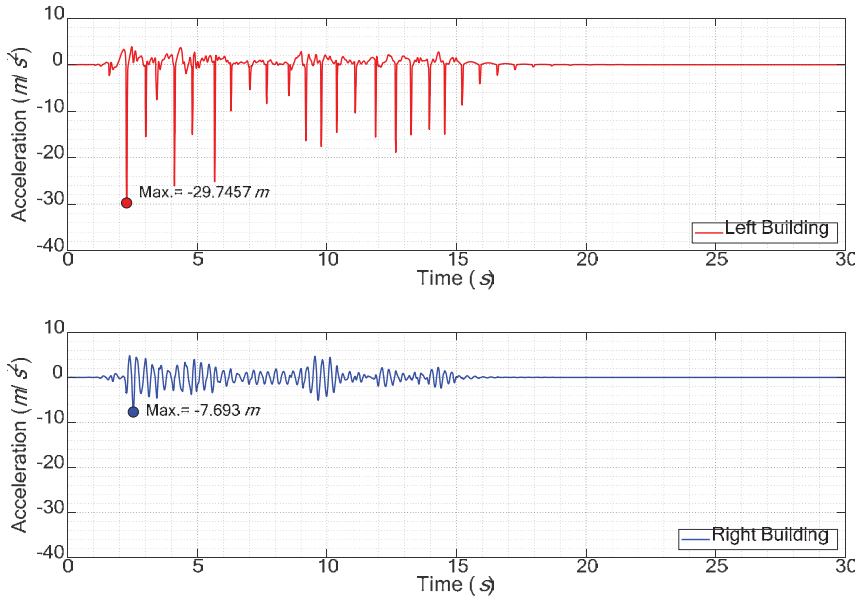

Figure 14: Acceleration time-history responses for the elastic case of the structural systems with no space in between.

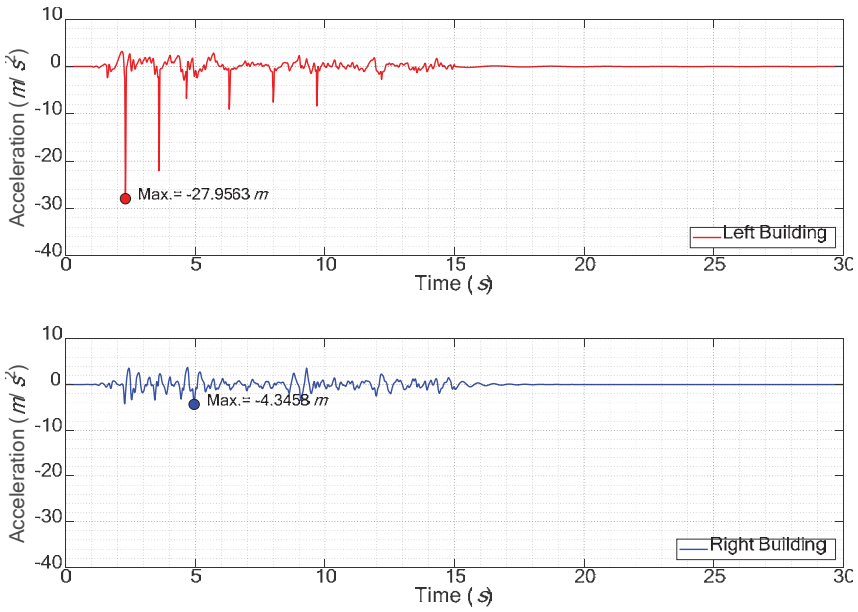

Figure 15: Acceleration time-history responses for the inelastic case of the structural systems with no space in between.

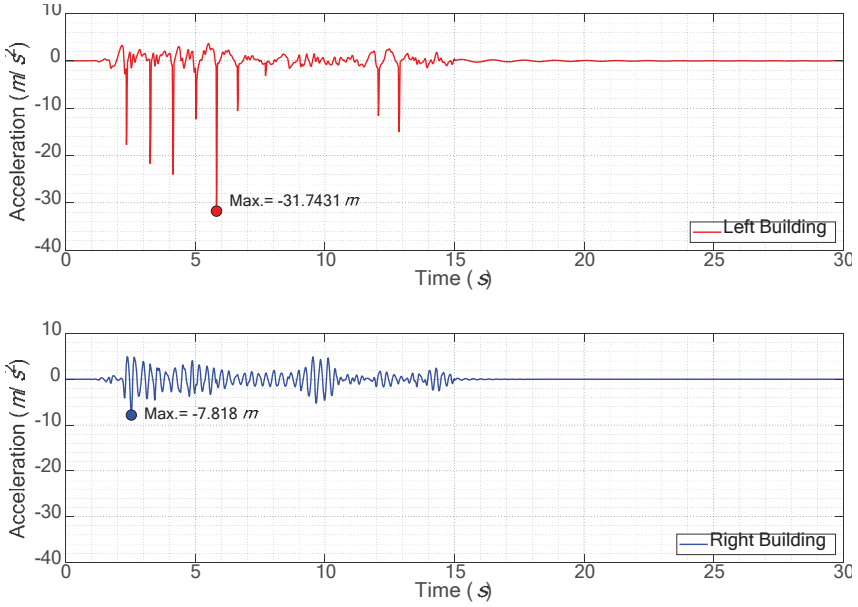

Figure 16: Acceleration time-history responses for the elastic case of the structural systems separated by a distance of 3 *cm*.

Figure 11 shows the pounding cycles that display the reduced number of cycles and the relatively small magnitude of impacts in the inelastic case. The influence of the gap size when inelastic behavior is considered can also be seen in the graphs of Figures 12 and 13 in which in the right building corresponding to the stiffer structure there is no clear difference between the responses with and without pounding. On the contrary, the flexible structure exhibits clear increases in the rebound displacements and hysteresis energy dissipation as well as the presence of permanent deformations which increase for smaller gap sizes.

Single-degree-of-freedom structural systems with elastic and inelastic behavior were considered in this study and the differences between these were addressed. Although it should be pointed out that further research is required to better investigate this complex behavior with

building pounding that should include more degrees of freedom, three-dimensional analysis including tangential/friction forces, different ground motion excitations, parametric and sensitivity analysis to understand the influence of intervenient input parameters on the output responses, presence of non-structural elements such as infill walls which are common in building structures, and the consideration of different pounding scenarios.

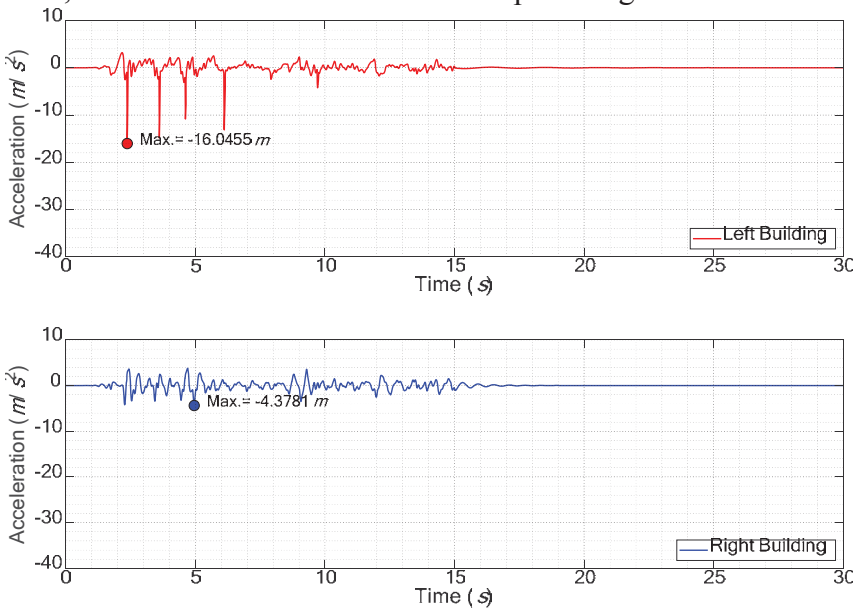

Figure 17: Acceleration time-history responses for the inelastic case of the structural systems separated by a distance of 3 *cm*.

Behavior of frame structure	Gap (*cm*)	Peak absolute values							N° of impacts
		x_L (*m*)	x_R (*m*)	$\dot{x}_L$ (*m/s*)	$\dot{x}_R$ (*m/s*)	$\ddot{x}_L$ (m/s^2)	$\ddot{x}_R$ (m/s^2)	F_P (*kN*)	
Linear Elastic	15	0.118	0.133	0.598	-0.312	-4.588	-7.961	0	0
	10	0.094 (-20%)	0.013 (-90%)	0.579 (-3%)	-0.312 (0%)	-13.837 (202%)	-7.961 (0%)	683.72	2
	5	-0.124 (5%)	0.013 (-90%)	0.694 (16%)	-0.312 (0%)	-29.877 (551%)	-7.961 (0%)	2077.7	4
	3	-0.110 (-6%)	0.013 (-90%)	0.704 (18%)	-0.309 (-1%)	-31.743 (592%)	-7.818 (-2%)	2315.8	9
	0	-0.106 (-10%)	-0.044 (-67%)	-0.589 (-1%)	-0.296 (-5%)	-29.746 (548%)	-7.693 (-3%)	2069	29
Non-linear Inelastic	15	-0.117	0.017	0.424	-0.276	-3.274	-4.447	0	0
	5	-0.120 (3%) (-4%)	0.017 (0%) (28%)	0.423 (0%) (-39%)	-0.277 (0%) (-11%)	-12.070 (269%) (-60%)	-4.449 (0%) (-44%)	849.87 (-59%)	2 (-50%)
	3	-0.157 (34%) (42%)	0.017 (-2%) (28%)	0.467 (10%) (-34%)	-0.271 (-2%) (-12%)	-16.046 (390%) (-49%)	-4.378 (-2%) (-44%)	1149.3 (-50%)	6 (-33%)
	0	-0.202 (73%) (90%)	-0.029 (69%) (-34%)	-0.573 (35%) (-3%)	-0.269 (-3%) (-9%)	-27.956 (754%) (-6%)	-4.346 (-2%) (-44%)	1924.1 (-7%)	10 (-66%)

a. The percentage below the values in blue color stands for the absolute percentage of increase or decrease regarding the case with no pounding.
b. The percentage below the values in green color stands for the absolute percentage of increase or decrease regarding the corresponding linear elastic behavior case.

Table 2: Relevant results of the simulations carried out.

6 CONCLUSIONS

The present study concerns earthquake-induced structural building pounding considering two SDOF systems with elastic and inelastic behavior. Building pounding can be simulated by the use of impact models which rely on the proper establishment of its parameters. Several analytical expressions were provided to calculate each of the parameters of the impact models which depend essentially on the impact stiffness, impact damping, and coefficient of restitution. The uncertainties regarding these parameters are intrinsically connected with the over-simplified assumptions considered as well as the unknown geometry and material properties of the contact region. Experimental data and parametric sensitivity studies may reduce the level of uncertainties and/or redirect the investigations for particular input parameters to obtain more reliable results.

One of the factors that may influence pounding-involved results is the consideration of the inelastic behavior of the colliding structures. Pounding forces caused permanent damage on the buildings in the rebound direction, especially in the flexible structure, increasing for smaller gap sizes. In addition, it was observed that the inelastic behavior should be considered since the most flexible structure presents higher increases of displacements when pounding is considered, and the acceleration spikes continue to have large peak values. The positive effect is the reduction of the number of impacts and their intensity compared with the elastic case. Hence, the neglection of the structural inelastic behavior may overestimate the magnitude of pounding forces and underestimate the displacement amplitude as well as neglect the permanent deformations that will certainly arise during earthquakes.

Further research is necessary since it is not possible to find a clear pattern or trend in the results concerning the input parameters and the desired output results using only SDOF systems with representative inelastic behavior under a specific ground motion. Future studies should address more degrees of freedom and possibly a three-dimensional spatial model (to account for forces in the tangential direction), calibration of the hysteresis model with experimental data, and the consideration of several different ground motions to validate the presented results as well and contribute with additional information on the matter of earthquake-induced structural building pounding.

ACKNOWLEDGEMENTS

This paper is within the scope of the first author's Ph.D. degree in progress, financially supported by the Portuguese Foundation for Science and Technology (FCT) through the PhD grant reference SFRH/BD/139570/2018 under the programme POCH (N2020 – P2020) and subsidized by the European Social Fund (FSE) and national funds from MCTES. This work was financially supported by: Base Funding - UIDB/04708/2020 of the CONSTRUCT - Instituto de I&D em Estruturas e Construções - funded by national funds through the FCT/MCTES (PIDDAC).

REFERENCES

[1] N. Mate, S. Bakre, O. Jaiswal and K. Sayyad, "Elastic and Inelastic Response of Structural Systems in Seismic Pounding," *Open Journal of Civil Engineering*, vol. 6, pp. 50-73, 2016.

[2] N. Mate, S. Bakre and O. Jaiswal, "Seismic Pounding Response of Singled-Degree-of-Freedom Elastic and Inelastic Structures Using Passive Tuned Mass Damper," *International Journal of Civil Engineering,* vol. 15, pp. 991-1005, 2017.

[3] Bouc, R. “Forced vibration of mechanical systems with hysteresis”. Proceedings of the Fourth Conference on Non-linear oscillation. Prague, Czechoslovakia. 1967.

[4] Bouc, R. “Modele mathematique d'hysteresis et application aux systems un degre de liberte”. These de Doctorat. Marseille, France. 1969.

[5] Bouc, R. “Modele mathematique d'hysteresis”. Application au circuit oscillant self saturable. Cinquieme Congres Oscillations Non-Lineaires. Volume 4, pp. 100-112. Kiev, Ukraine 1969.

[6] Bouc, R. “Modele mathematique d'hysteresis. Acustica”. Volume 24, pp. 16-25. 1971.

[7] Y.-K. Wen, “Method for Random Vibration of Hysteretic Systems,” *Journal of the Engineering Mechanics Division, ASCE,* vol. 102, no. 2, pp. 249-263, 1976.

[8] Y.-K. Wen, “Equivalent Linearization for Hysteretic System under Random Excitation,” *Journal of Applied Mechanics, ASME,* vol. 47, no. 1, pp. 150-154, 1980.

[9] T. T. Baber and Y.-K. Wen, “Random Vibration of Hysteretic, Degrading Systems,” *Journal of the Engineering Mechanics Division, ASCE,* vol. 107, no. 6, pp. 1069-1087, 1981.

[10] T. T. Baber and M.-N. Noori, “Random Vibration of Degrading Pinching Systems,” *Journal of the Engineering Mechanics Division, ASCE,* vol. 11, no. 8, pp. 1010-1026, 1985.

[11] T. T. Baber and M.-N. Noori, “Modeling General Hysteresis Behavior and Random Vibration Application,” *Journal of Vibration, Acoustic, Stress, and Reliability in Design, ASME,* vol. 108, no. 4, pp. 411-420, 1986.

[12] G. C. Foliente, “Hysteresis Modeling of Wood Joints and Structural Systems,” *Journal of Structural Engineering, ASCE,* vol. 121, no. 6, pp. 1013-1022, 1995.

[13] M. V. Sivaselvan and A. M. Reinhorn, “Hysteretic Models for Cyclic Behavior of Deteriorating Inelastic Structures,” Technical Report MCEER-99-0018, Multidisciplinary Center for Earthquake Engineering Research, State University of New York at Buffalo, Buffalo, New York, 1999.

[14] M. V. Sivaselven and A. M. Reinhorn, “Hysteretic models for deteriorating inelastic structures,” *Journal of Engineering Mechanics,* vol. 126, no. 6, pp. 633-640, 2000.

[15] R. Jankowski and S. Mahmoud, Earthquake-Induced Structural Pounding, Switzerland: Springer, 2015.

[16] Goldsmith, W. Impact: The Theory and Physical Behaviour of Colliding Solids. Edward Arnold (Publishers) LTD: London. 1960.

[17] R. Jankowski, “Experimental study on earthquake-induced pounding between structural elements made of different building materials,” *Earthquake Engineering and Structural Dynamics*, vol. 39, pp. 349-354, 2010.

[18] M. Mahmoud, K. Choong, and R. Jankowski, “Seismic pounding between adjacent buildings: Identification of parameters, soil interaction issues and mitigation measures,” *Soil Dynamics and Earthquake Engineering*, vol. 121, pp. 135-150, 2019.

[19] K. Johnson, “Contact Mechanics,” Cambridge university press, 1987.

[20] H. Hertz, "Über die Berührung fester elastischer Körper (On the contact of elastic solids)," *J. für die Reine und Angewandte Mathematik,* vol. 29, pp. 156-171, 1881. (in German)

[21] J. Wolf and P. Skrikerud, "Mutual pounding of adjacent structures during earthquakes," *Nuclear Engineering and Design*, vol. 57, pp. 253-275, 1980.

[22] S. Anagnostopoulos, "Pounding of buildings in series during earthquakes," *Earthquake* Engineering and Structural Dynamics, vol. 16, pp. 443-456, 1988.

[23] S. Anagnostopoulos, "Equivalent viscous damping for modeling inelastic impacts in earthquake pounding problems," *Earthquake Engineering and Structural Dynamics*, vol. 33, pp. 897-902, 2004.

[24] P. Komodromos, P. Polycarpou, L. Papaloizo, and M. Phocas, "Response of seismically isolated buildings considering poundings," *Earthquake Engineering and Structural Dynamics*, vol. 36, pp. 1605-1622, 2007.

[25] R. Valles and A. Reinhorn, "Evaluation, prevention and mitigation of pounding effects in building structures," Technical Report NCEER-97-0001, *National Center for Earthquake Engineering Research*, State University of New York, Buffalo, USA, 1997.

[26] S. Mahmoud, "Modified linear viscoelastic model for elimination of the tension force in the linear viscoelastic," in *The Fourteenth World Conference on Earthquake Engineering, October 12-17, 2008,* Beijing, China, 2008.

[27] R. Jankowski, "Analytical expression between the impact damping ratio and the coefficient of restitution in the non-linear viscoelastic model of structural pounding," *Earthquake Engineering and Structural Dynamics*, vol. 35, pp. 517-524, 2006.

[28] K. Ye, L. Li and H. Zhu, "A modified Kelvin impact model for pounding simulation of base-isolated building with adjacent structures," *Earthquake Engineering and Engineering Vibration*, vol. 8, pp. 433-446, 2009.

[29] D. Pant, A. Wijeyewickrema and T. Ohmachi, "Three dimensional nonlinear analysis of seismic pounding between multi-story reinforced concrete buildings," in *Proceedings of the Seventh International Conference on Urban Earthquake Engineering (7CUEE) and Fifth International Conference on Earthquake Engineering (5ICEE)*, Vol II: 1829-1840, 2010.

[30] D. Pant, A. Wijeyewickrema and T. Ohmachi, "Seismic Pounding between Reinforced Concrete Buildings: A Study using two recently proposed Contact Element Models," in *Proceeding of the 14th European Conference on Earthquake Engineering, European Conference on Earthquake Engineering*, Republic of Macedonia, 2010.

[31] S. Mahmoud and R. Jankowski, "Modified linear viscoelastic model of earthquake-induced structural pounding," *Iranian Journal of Science and Technology*, vol. 35, no. C1, pp. 51-62, 2011.

[32] H. Lankarani and P. Nikravesh, "A Contact Force Model With Hysteresis Damping for Impact Analysis of Multibody Systems," *Journal of Mechanical Design*, vol. 112, pp. 369-376, 1990.

[33] H. Lankarani and P. Nikravesh, "Continuous Contact Force Models for Impact Analysis in Multibody Systems," *Nonlinear Dynamics*, vol. 5, pp. 193-207, 1994.

[34] K. Hunt and F. Crossley, "Coefficient of restitution interpreted as damping in vibroimpact," *Journal of Applied Mechanics, American Society of Mechanical Engineers,* vol. 42, pp. 440-445, 1975.

[35] S. Muthukumar, "A contact element approach with hysteresis damping for the analysis and design of pounding in bridges," Ph.D. Thesis, Georgia Institute of Technology, Georgia, EUA, 2003.

[36] S. Muthukumar and R. DesRoches, "A Hertz contact model with non-linear damping for pounding simulation," *Earthquake Engineering and Structural Dynamics,* vol. 35, pp. 811-829, 2006.

[37] R. Jankowski, "Non-linear viscoelastic modelling of earthquake-induced structural pounding," *Earthquake Engineering and Structural Dynamics,* vol. 34, pp. 595-611, 2005.

[38] K. Ye, L. Li and H. Zhu, "A note on the Hertz contact model with nonlinear damping for pounding simulation," *Earthquake Engineering and Structural Dynamics*, vol. 38, pp. 1135-1142, 2009.

[39] H. Naderpour, R. Barros, and S. Khatami, "A new model for calculating impact force and energy dissipation based on the CR-factor and impact velocity," Scientia Iranica A, vol. 22, pp. 59-68, 2015.

[40] H. Naderpour, R. Barros, R. Khatami, and R. Jankowski, "Numerical Study on Pounding between Two Adjacent Buildings under Earthquake Excitation," *Hindawi Publishing Corporation: Shock and Vibration*, vol. 2016, 2016.

[41] F. Bamer, "A Hertz-pounding formulation with a nonlinear damping and a dry friction element," *Acta Mechanica*, vol. 229, pp. 4485-4494, 2018.

[42] F. Bamer and B. Markert, "A nonlinear visco-elastoplastic model for structural pounding," *Earthquake Engineering and Structural Dynamics,* vol. 47(12), pp. 2490-2495, 2018.

[43] F. Bamer, N. Strubel, J. Shi and B. Markert, "A visco-elastoplastic pounding damage formulation*," Engineering Structures*, vol. 197, 2019.

[44] S. Khatami, H. Naderpour, R. C. Barros, A. Jakubczyk-Gałczynska and R. Jankowski, "Effective Formula for Impact Damping Ratio for Simulation of Earthquake-induced Structural Pounding," *Geosciences, MDPI,* vol. 9, no. 8: 347, 2019.

[45] J. van Mier, A. F. Pruijssers, H. Reinhardt and T. Monnier, "Load-Time Response of Colliding Concrete Bodies," Journal of Structural Engineering, Vols. 117, No. 2, no. 25544, pp. 354-374, 1991.

[46] K. Chau, X. Wei, X. Guo and C. Shen, "Experimental and theoretical simulations of seismic poundings between two adjacent structures," *Earthquake Engineering and Structural Dynamics*, vol. 32, pp. 537-554, 2003.

[47] M. Goland, P. Wickersham, and M. Dengler, "Propagation of elastic impact in beams in bending," *Journal of Applied Mechanics*, vol. 22, pp. 1-7, 1955.

[48] P. Zhu, M. Abe, and Y. Fujino, "Modelling three-dimensional non-linear seismic performance of elevated bridges with emphasis on pounding of girders," *Earthquake Engineering and Structural Dynamics*, vol. 31, pp. 1891-1913, 2002.

[49] Y. Kajita, T. Kitahara, Y. Nishimoto, and H. Otsuka, "Estimation of Maximum Impact Force on Natural Rubber during Collision of Two Steel Bars," In Proceedings of the First European Conference on Earthquake Engineering and Seismology (1st ECEES), Geneva, Switzerland, 3–8 September 2006; p. 488.

[50] P. Polycarpou, L. Papaloizou, P. Komodromos, "An efficient methodology for simulating earthquake-induced 3D pounding of buildings", *Earthquake Engineering and Structural Dynamics*, vol. 43, pp. 985–1003, 2014.

[51] G. L. Cole, R. P. Dhakal, A. J. Carr and D. K. Bull, "Building pounding state of the art: Identifying structures vulnerable to pounding damage," in *New Zealand Society of Earthquake Engineerings (NZSEE) Conference, 26-28 March*, Wellington, NZ, 2010.

[52] MATLAB 2014a., Natick, Massachusetts, USA: MathWorks, Inc., 2014.

[53] Pacific Earthquake Engineering Research Center (PEER) strong ground motion database, [Online]. Available: https://peer.berkeley.edu/peer-strong-ground-motion-databases.